
ADVERSARIAL REINFORCEMENT LEARNING FRAMEWORK FOR ESP CHEATER SIMULATION

**Inkyu Park¹, Jeong-Gwan Lee¹, Taehwan Kwon¹,
Juheon Choi², Seungku Kim², Junsu Kim², Kimin Lee²**
¹KRAFTON, ²KAIST

ABSTRACT

Extra-Sensory Perception (ESP) cheats, which reveal hidden in-game information such as enemy locations, are difficult to detect because their effects are not directly observable in player behavior. The lack of observable evidence makes it difficult to collect reliably labeled data, which is essential for training effective anti-cheat systems. Furthermore, cheaters often adapt their behavior by limiting or disguising their cheat usage, which further complicates detection and detector development. To address these challenges, we propose a simulation framework for controlled modeling of ESP cheaters, non-cheaters, and trajectory-based detectors. We model cheaters and non-cheaters as reinforcement learning agents with different levels of observability, while detectors classify their behavioral trajectories. Next, we formulate the interaction between the cheater and the detector as an adversarial game, allowing both players to co-adapt over time. To reflect realistic cheater strategies, we introduce a structured cheater model that dynamically switches between cheating and non-cheating behaviors based on detection risk. Experiments demonstrate that our framework successfully simulates adaptive cheater behaviors that strategically balance reward optimization and detection evasion. This work provides a controllable and extensible platform for studying adaptive cheating behaviors and developing effective cheat detectors.

1 INTRODUCTION

Cheating is a persistent issue in digital games that significantly violates the fairness and degrades the user experience. If cheating is not properly addressed, it may drive players away from the game, ultimately leading to reduced revenue for game developers. It has been reported to cause an estimated loss of \$29 billion and to drive away 78% of gamers for a year (Irdeto, 2022).

One of the most representative forms of cheating is Extra-Sensory Perception (ESP), which allows cheaters to access hidden game information. A common example is the use of wallhacks in first-person shooter (FPS) games: while normal players cannot see opponents behind walls, cheaters can, enabling them to avoid unexpected attacks and easily eliminate enemies. These unfair advantages severely disrupt the balance of the game, especially in settings where players must make decisions and formulate strategies based on incomplete information. ESP cheats are notoriously hard to prevent due to their passive nature: they do not modify game files or client-side data. In addition, their usage is often indistinguishable from normal gameplay when observed from a third-person perspective, making them especially challenging to detect through in-game monitoring or user reports (PUBG: BATTLEGROUNDS Anti-Cheat Team, 2024).

Another major challenge in detecting ESP cheats is the lack of a reliable dataset for developing anti-cheat systems. First, it is hard to clearly distinguish between cheaters and non-cheaters. Cheaters may adopt various strategies: some use cheats consistently throughout a game, some toggle them on and off, while others behave as if they are not cheating - taking suboptimal actions or mimicking normal gameplay - to avoid suspicion. Moreover, they may also pretend their advantageous actions are coincidences in order to appear as normal players. Because of these strategies, even with monitoring, it is difficult to judge whether a player is actually cheating or just getting lucky. Sometimes, non-cheaters with unusually good luck are falsely flagged as cheaters and punished. Even when penalties are imposed, it is very rare for players to admit that they used cheats. As a result, a significant number of cases can be mislabeled.

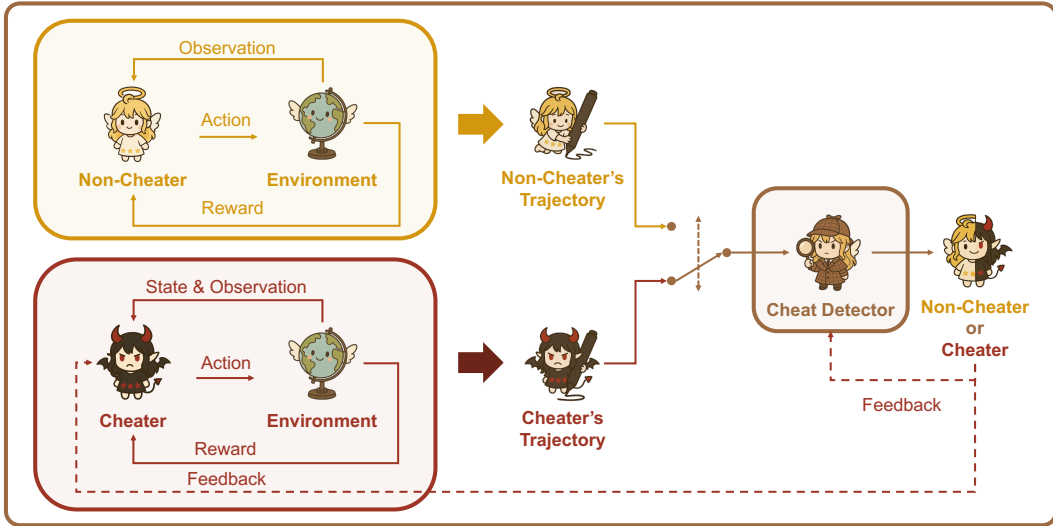


Figure 1: Overview of ESP cheater simulation framework. The cheat detector discriminates the trajectory whether it was generated by a non-cheater or a cheater. After detector making its decision, the cheater updates its policy based on the detection result in order to evade detection. Simultaneously, the cheat detector updates itself to improve its classification accuracy.

Next, cheaters continuously evolve their strategies to evade detection (Tao et al., 2018; Jonnalagadda et al., 2021). When a cheat detector is developed and deployed, cheaters adapt by limiting their cheat usage just enough to avoid detection. For example, if a simple threshold-based detection algorithm is used, cheaters will intentionally operate just below the threshold to remain undetected. As a result, the statistical characteristics of past cheater data differ from those of recent data. Since only recent data is useful for developing effective detectors, it becomes difficult to collect a large amount of high-quality training and test data.

Due to these challenges, constructing a reliable real-world dataset is difficult. It hinders the development and evaluation of cheat detectors that are both trustworthy and high-performing. To address these limitations, we adopt simulation as an alternative approach. Simulation offers several key advantages. First, it provides full control over the environment, allowing us to assign ground-truth labels with complete certainty. Second, simulation can be scaled as needed, allowing us to generate a large amount of training data to support robust detector development. Last, simulation enables us to reproduce and study various cheating strategies mentioned earlier, providing a controlled way to train detectors against diverse and sophisticated behaviors.

To this end, we introduce the ESP simulation framework that simulates cheaters, non-cheaters, and cheat detectors with their co-evolving behaviors. In the partially observable environment, we model the cheater and the non-cheater as reinforcement learning (RL) agents with different levels of observability. We use a classifier as a cheat detector to estimate the probability of a trajectory being generated by the cheater. We formulate the interaction between players as a minimax problem, enabling both to co-evolve during training. An overview of the framework is illustrated in Fig. 1.

To verify the effectiveness of the framework, we implement *Gridworld* and *Blackjack* environments that can simulate both fully observable and partially observable agents. We also use various designs of the detector based on the trajectory, the trajectory length, and the reward. With these diverse configurations, we conduct extensive experiments, demonstrating the effectiveness of our framework in modeling adaptive cheaters. Our code is available at <https://github.com/yunik1004/esp-simulator>.

2 RELATED WORKS

Cheat Detection for Games. Several studies (Alayed et al., 2013; Tao et al., 2018; Jonnalagadda et al., 2021; Pinto et al., 2021; Kanervisto et al., 2022; Zhang et al., 2024) have explored cheat detection in video games, proposing a variety of approaches for identifying different types of malicious behaviors. Alayed et al. (2013) used a support vector machine (SVM) (Suthaharan, 2016) to detect

aimbots based on server-side logs from online FPS games. Tao et al. (2018) proposed NGUARD, a bot detection framework for multiplayer online role-playing games (MMORPGs), which combines supervised and unsupervised learning to detect known bots and discover previously unseen ones. Jonnalagadda et al. (2021) introduced a vision-based deep neural network (DNN) detector to identify illicit on-screen overlays in *Counter-Strike: Global Offensive* (CS:GO) (Valve, 2012). In addition, they applied the interval bound propagation method (Gowal et al., 2018) to defend against adversarial attacks targeting the detection system. Pinto et al. (2021) formulated sequences of keyboard and mouse events as a multivariate time series, and employed a convolutional neural network (CNN) (O’shea & Nash, 2015) to detect triggerbots and aimbots in CS:GO. Kanervisto et al. (2022) developed an aimbot that mimics human behavior using a generative adversarial network (GAN) (Goodfellow et al., 2020), and evaluated the performance of multiple detection methods against it. Zhang et al. (2024) proposed HAWK, an anti-cheat framework for CS:GO, which leverages machine learning to mimic the decision process of human experts in detecting wallhacks and aimbots. Despite recent advances, most approaches assume that cheaters behave in fixed, non-adaptive ways. It overlooks the fact that real-world cheaters often adjust their strategies to avoid detection, highlighting the need for simulation frameworks that can model such adaptive behaviors.

Adversarial Training in Reinforcement Learning. Adversarial learning traces its roots to the GAN (Goodfellow et al., 2020), where a generator and a discriminator engage in a minimax game to match data distributions. Ho & Ermon (2016) later carried this game-theoretic structure over to reinforcement learning with *generative adversarial imitation learning* (GAIL), which trains a policy to fool a discriminator that separates expert and learner trajectories, thereby reproducing the expert’s state–action occupancy without an explicit reward-recovery step. For *robustness*, Pinto et al. (2017) proposed *robust adversarial reinforcement learning* (RARL), where an adversary injects disturbance forces into the simulator so that the resulting policy remains stable under variations in friction, mass, and other model mismatches. Dennis et al. (2020) later introduced *protagonist–antagonist induced regret environment design* (PAIRED), training an environment designer and an antagonist demonstrator to build a curriculum of tasks that are solvable yet currently unsolved by the protagonist, thereby boosting zero-shot transfer. Although these lines of work pursue diverse goals in imitation (Ho & Ermon, 2016), robustness (Pinto et al., 2017), curriculum-driven generalization (Dennis et al., 2020), and domain expansion (Cheng et al., 2025), they all leverage adversarial interaction to enhance policy capability. In contrast, our framework jointly trains an ESP cheater and a trajectory-level detector in a partially observable setting, exploiting dynamic cheating behavior that balances reward optimization and detection evasion.

3 ESP SIMULATION FRAMEWORK

We model the game environment as a partially observable Markov decision process (POMDP) (Åström, 1965; Kaelbling et al., 1998), defined by the tuple $\langle \mathcal{S}, \mathcal{A}, T, r, \Omega, O, \gamma \rangle$, where \mathcal{S} is the set of environment states, \mathcal{A} is the set of actions, T denotes the state transition probability distribution, $r : \mathcal{S} \times \mathcal{A} \rightarrow \mathbb{R}$ is the reward function, Ω is the set of observations available to the non-cheater player, O is the observation function, defining the conditional observation probabilities, and $\gamma \in [0, 1]$ is a discount factor. Consistent with previous works related to the trajectory feedback (Liu et al., 2019; Efroni et al., 2021), we assume $\gamma = 1$ throughout this paper.

We consider three different players in this game: the ESP cheater, the non-cheater, and the cheat detector. To simplify the problem, we make the following assumptions:

1. There is only a single cheater, a single non-cheater, and a single cheat detector.
2. Given a trajectory, a sequence of states and actions $\tau = (s_1, a_1, s_2, a_2, \dots, s_t, a_t)$, the detector estimates the probability that it was generated by the cheater. During the inference, the detector receives no information about the ground-truth label of the trajectory. On the other hand, it is allowed to access the ground-truth label during the training.
3. The non-cheater operates under partial observability. On the other hand, the ESP cheater has full observability of the environment and can directly access the state. The cheater also has access to the observations available to the non-cheater, as well as the cheater probability assigned by the detector to its generated trajectory.

4. Players are bounded rational (Simon, 1955; Kahneman & Tversky, 1982; Selten, 1990). According to the concept of the bounded rationality, decision makers often struggle to find a global optimum due to their limited information, time, and computational resources. As a result, they remain at a nearby local optimum. Experimental studies (Nagel, 1995; Coricelli & Nagel, 2009) also support this claim by showing that players in games do not act rationally and their behavior is bounded. From a game theory perspective (Flåm, 1998; Chen et al., 2011; Ratliff et al., 2016), this implies that players tend to reach the local Nash equilibrium (Alos-Ferrer & Ania, 2001) and rarely shift to the different local optimal strategy.

Under these assumptions, the non-cheater uses the policy $\pi_n : \Omega \times \mathcal{A} \rightarrow [0, 1]$, the cheater uses the policy $\pi_c : \mathcal{S} \times \Omega \times \mathcal{A} \rightarrow [0, 1]$, and the cheat detector uses the classifier $D : \mathcal{T} \rightarrow [0, 1]$, where \mathcal{T} denotes the set of all possible trajectories. Since the non-cheater follows the local optimal policy under partial observability, π_n can be obtained by solving a reward maximization problem $\max_{\pi_n} J(\pi_n)$ with policy optimization algorithms such as A2C (Mnih et al., 2016) and PPO (Schulman et al., 2017), where $J(\pi_n)$ denotes the expected return under policy π_n . Note that it is guaranteed to reach the local optimum when using temporal difference (Maei et al., 2009), deep Q-learning (Fan et al., 2020), and actor-critic methods (Holzleitner et al., 2021; Tian et al., 2023).

Next, we formulate the dynamic interaction between the ESP cheater and the detector as an adversarial game. In this setup, the detector aims to improve its classification performance by analyzing behavior patterns exhibited by the agents, while the cheater continually adapts its strategy to evade detection and maximize in-game rewards. Formally, the detector updates its classifier D to distinguish between trajectories induced by the cheater policy π_c and the non-cheater policy π_n , by minimizing the binary cross-entropy loss over samples $\tau_c \sim \pi_c$ and $\tau_n \sim \pi_n$. Simultaneously, the cheater optimizes its policy π_c to maximize the expected return $J(\pi_c)$ while minimizing $D(\tau_c)$, thereby reducing the classifier's confidence in identifying cheating behaviors. It is formalized as a minimax game:

$$\min_{\pi_c} \max_D \mathbb{E}_{\tau_c \sim \pi_c} [\log D(\tau_c)] + \mathbb{E}_{\tau_n \sim \pi_n} [\log(1 - D(\tau_n))] - \lambda^{-1} J(\pi_c), \quad (1)$$

where $\lambda \geq 0$ is an adversarial coefficient. It is a hyperparameter that controls the trade-off between maximizing in-game rewards and minimizing detector's detectability.

To find the local Nash equilibrium, we employ an alternating optimization approach with the gradient descent-ascent (GDA) algorithm, in which the cheater policy π_c and the classifier D are iteratively trained. Specifically, equation 1 can be decomposed into two sub-problems:

$$\text{Optimize cheater policy : } \max_{\pi_c} J(\pi_c) - \lambda \mathbb{E}_{\tau_c \sim \pi_c} [\log D(\tau_c)] \quad (2)$$

$$\text{Optimize cheat detector : } \max_D \mathbb{E}_{\tau_c \sim \pi_c} [\log D(\tau_c)] + \mathbb{E}_{\tau_n \sim \pi_n} [\log(1 - D(\tau_n))]. \quad (3)$$

Note that Daskalakis & Panageas (2018); Adolphs et al. (2019); Mazumdar et al. (2020) theoretically proved that applying GDA to a minimax problem yields a local Nash equilibrium.

In practice, $\log D$ in equation 2 may not provide sufficiently strong gradients for effective optimization of π_c , as discussed in Goodfellow et al. (2020). When the classifier becomes confident in its predictions, $\log D(\tau)$ tends to saturate, thereby diminishing its influence on the objective. To alleviate this issue, we adopt $-\log(1 - D(\tau))$ in place of $\log D(\tau)$, as suggested in Goodfellow et al. (2020). It yields the following surrogate objective:

$$\text{Optimize cheater policy (Practical) : } \max_{\pi_c} J(\pi_c) + \lambda \mathbb{E}_{\tau_c \sim \pi_c} [\log(1 - D(\tau_c))]. \quad (4)$$

To solve the equation 4, we apply reward shaping (Ng et al., 1999) with the shaped reward r'_t :

$$r'_t = \begin{cases} r_t, & \text{if } t < |\tau_c| - 1 \\ r_t + \lambda \log(1 - D(\tau_c)), & \text{if } t = |\tau_c| - 1, \end{cases} \quad (5)$$

where r_t denotes the original reward at timestep t . This transformation reformulates the objective in equation 4 into a standard expected return form $\mathbb{E}[\sum_t r'_t]$ as follows:

$$J(\pi_c) + \lambda \mathbb{E}_{\tau_c \sim \pi_c} [\log(1 - D(\tau_c))] = \mathbb{E}_{\tau_c \sim \pi_c} [\sum_t r_t + \lambda \log(1 - D(\tau_c))] = \mathbb{E}_{\tau_c \sim \pi_c} [\sum_t r'_t]. \quad (6)$$

It enables the use of standard policy optimization algorithms, such as A2C, PPO and others.

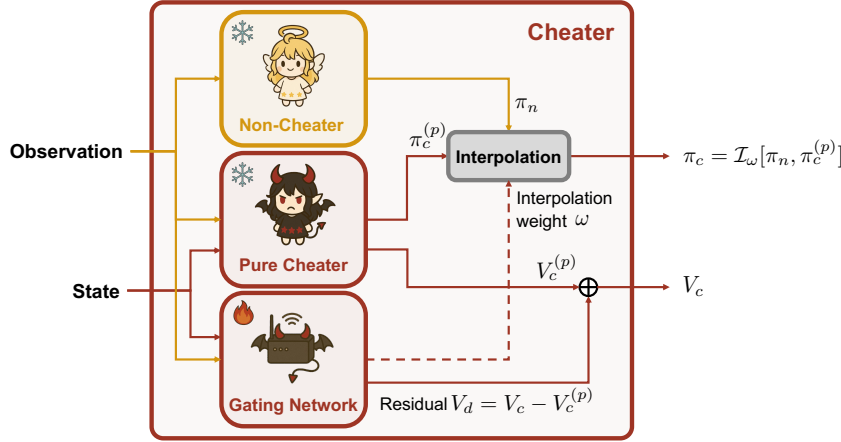


Figure 2: Actor-critic model architecture of the cheater. The model consists of three components: the non-cheater, the pure cheater, and the gating network. Only the gating network is trainable. The gating network produces an interpolation weight ω used to combine the two policies, as well as the residual value $V_d = V_c - V_c^{(p)}$ corresponding to the expected penalty by the detector.

Structured Cheater Modeling. In actual gameplay, cheaters rarely invent new tactics. They tend to behave like non-cheaters most of the time and exploit cheating only at critical moments to gain a decisive advantage. In other words, a realistic cheater behaves as a mixture of a non-cheater and a pure cheater, which represents the local optimal agent under full observability without any constraints related to detectability.

To reflect this behavior, we model the cheater policy π_c as an interpolation of the non-cheater policy π_n and the pure cheater policy $\pi_c^{(p)}$: $\mathcal{S} \times \Omega \times \mathcal{A} \rightarrow [0, 1]$:

$$\pi_c(a|s, o) = I_{\omega(s, o)}[\pi_n(a|o), \pi_c^{(p)}(a|s, o)], \quad (7)$$

where $\omega : \mathcal{S} \times \Omega \rightarrow [0, 1]$ denotes the interpolation weight function. In this paper, we adopt a linear interpolation: $\pi_c(a|s, o) = (1 - \omega(s, o)) \cdot \pi_n(a|o) + \omega(s, o) \cdot \pi_c^{(p)}(a|s, o)$. Similar to the non-cheater policy, the pure cheater policy can be obtained by solving reward maximization problem $\max_{\pi_c^{(p)}} J(\pi_c^{(p)})$ with policy optimization algorithms. ω acts as a routing function, controlling the degree to which the agent behaves like a cheater. It is a learnable function, enabling the agent to adaptively decide when to cheat based on the current state and observation. It allows the cheater policy to interpolate smoothly between cheating and non-cheating behaviors based on context.

Next, we can use the value function $V_c^{(p)}$ of the pure cheater as an initial point to train the value function V_c of the cheater. Specifically, we decompose the value function V_c into two parts: $V_c^{(p)}$ estimates the return expected under the pure cheater policy, while the residual $V_d = V_c - V_c^{(p)}$ serves as an auxiliary component that accounts for the potential penalty associated with detection risk and the value difference induced by the mixture of policies. V_d is modeled as a learnable function, allowing the agent to infer contextual detectability, account for the mixture of policies, and adjust its value estimate accordingly. We illustrate the detailed architecture of the cheater in Fig. 2. The full optimization process with the structured cheater modeling is provided in Algo. 1.

4 EXPERIMENTS

4.1 EXPERIMENT SETUP

Environments. To test the framework and the optimization algorithm described in Sec. 3, we design custom single-agent environments: *Gridworld* and *Blackjack*. Refer to Appendix A for the detailed explanations about environments. The Gridworld (Fig. 3a) is a two-dimensional grid world with randomly distributed items, walls, and lava. The agent controls its orientation and position using three actions: *TurnLeft*, *TurnRight*, and *MoveForward*. By default, only a small square region

Algorithm 1 Adversarial training of cheater and cheat detector

Input: Non-cheater policy π_n , pure cheater policy $\pi_c^{(p)}$, initial cheat detector D and adversarial coefficient λ

Output: Cheater policy π_c and updated D

 Initialize interpolation weight function ω

 Initialize $\pi_c \leftarrow \mathcal{I}_\omega[\pi_n, \pi_c^{(p)}] \cdots (7)$

for iteration=1, 2, \cdots **do**

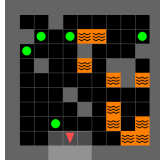
 Sample trajectories $\tau_c^i \sim \pi_c, \tau_n^i \sim \pi_n$

 Optimize ω by maximizing expected return with reward shaping (5) using $\{\tau_c^i\}$

 Optimize D by minimizing cross entropy (3) using $\{\tau_c^i\}$ and $\{\tau_n^i\}$

 Update $\pi_c \leftarrow \mathcal{I}_\omega[\pi_n, \pi_c^{(p)}] \cdots (7)$

end for



(a) Gridworld

Dealer	Player	Deck	Action
T♦, (3♣)	5♦, 3♦	6♣, (8♠), (2♠), (T♠), (9♦), (7♣), (9♣), (7♠), (6♥), (A♦), (6♠), (A♣), (A♥)	hit, stand

(b) Blackjack

Figure 3: (a) Visualization of the Gridworld environment. The figures show walls in gray, the agent as a red triangle, items as green circles, and lava as orange regions with black wave patterns. Only the 3×3 region in front of the agent is visible. (b) Visualization of the Blackjack environment. Cards with the parenthesis are invisible to the non-cheater.

in front of the agent is visible. On the other hand, the cheater agent can observe every grid. The agent receives a time-decaying reward when collecting the item and incurs a time-decaying penalty when encountering lava. The episode ends when the agent has collected all items or the maximum number of timesteps has elapsed. After the episode ends, the cheat detector receives the agent’s trajectory as form of image and discriminates whether the agent is a cheater or not.

The Blackjack (Fig. 3b) is a card game that the player aims to hold cards whose count does not exceed 21 while exceeding the dealer’s count. The player can use four actions to draw the card from the deck or to update the bet: *Hit*, *Stand*, *DoubleDown*, and *Surrender*. By default, the player can observe their hand (their initial hand + revealed cards from the deck) and the dealer’s upcard. In contrast, the cheater can observe every card, including the dealer’s hold card and the deck. After the episode ends, the player receives or loses the bet depending on their count. Then, the detector discriminates the cheater based on the trajectory including cards and the action history.

Evaluation Metrics. We employ three main metrics to evaluate the performances of the cheater and the detector: *Average precision (AP)*, *AUROC*, and *Average reward*. AP and AUROC evaluate the detector’s ability to distinguish cheater trajectories from non-cheater ones, while the average reward measures the effectiveness of the policy in the game environment. Lower AP and AUROC indicate that the cheater successfully deceives the detector. In addition, we report *Average trajectory length* to provide further insights into the agent behavior. Under the non-adversarial setting, non-cheaters tend to produce longer trajectories than cheaters, since they must actively explore the environment to search for items or check the next card, leading to longer episode length. Lastly, we use *Relative reward* to visualize the reward changes over detectability. It is defined as $(\text{reward} - \text{non-cheater's reward}) / (\text{pure cheater's reward} - \text{non-cheater's reward})$, to represent the normalized reward gain of the adversarial cheater compared to the pure cheater.

Implementation Details. We use a CNN-based actor-critic architecture for the policy network and a CNN-based classifier for the detector network. Both the cheater and non-cheater policies are trained using PPO algorithm (Schulman et al., 2017). Before conducting adversarial training, we construct the trajectory dataset for each policy and then pretrain the detector. The pretraining results are summarized in Tab. 1. For adversarial training, we finetune the cheater policy and the detector network based on Alg. 1. More details can be found in Appendix B.

Game	Player type	AP	AUROC	Average reward	Average trajectory length
Gridworld	Non-cheater	0.500 \pm 0.000	0.500 \pm 0.000	4.676 \pm 0.005	62.133 \pm 1.762
	Pure cheater	0.772 \pm 0.012	0.810 \pm 0.011	4.759 \pm 0.011	45.708 \pm 2.471
Blackjack	Non-cheater	0.500 \pm 0.000	0.500 \pm 0.000	-0.031 \pm 0.002	1.473 \pm 0.141
	Pure cheater	0.798 \pm 0.049	0.818 \pm 0.021	0.704 \pm 0.057	1.146 \pm 0.027

Table 1: Performances of the pretrained agents.

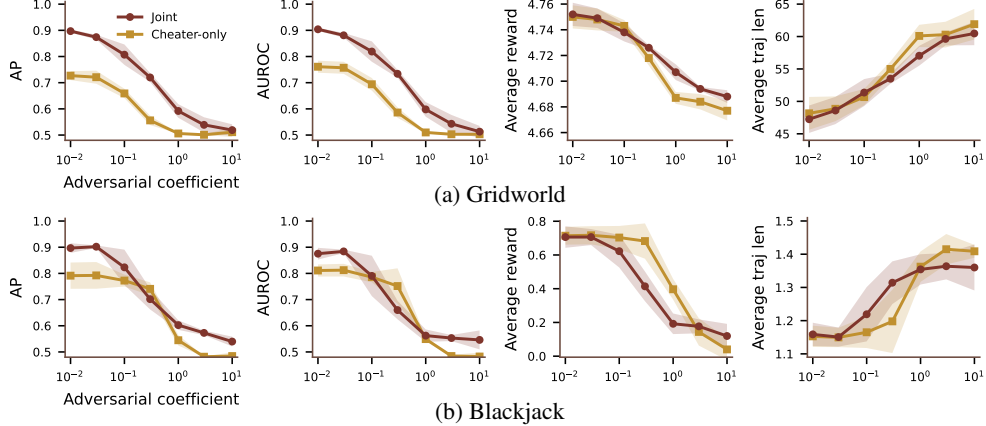


Figure 4: Performance metrics as functions of the adversarial coefficient λ . We plot the experimental results of two different settings: updating both the cheater and the detector (*Joint*) and updating only the cheater with the fixed detector (*Cheater-only*). As λ increases, the cheater becomes harder to detect (lower AP and AUROC). The average reward decreases gradually, showing that the cheater sacrifices efficiency to avoid detection. Average trajectory length increases as the cheater takes longer and less efficient choices to appear less suspicious.

4.2 ADVERSARIAL TRAINING

To validate the effectiveness of our adversarial simulation framework, we conduct the experiment to analyze how the cheater adapts its behavior under different detection pressures. We vary the adversarial coefficient λ in objective equation 4, which controls the trade-off between maximizing in-game rewards and minimizing the probability of being detected. The selected values for λ are 0.01, 0.03, 0.1, 0.3, 1, 3, and 10.

Fig. 4 presents quantitative results in an equilibrium under different values of λ . As λ increases, the cheater policy places more emphasis on deceiving the detector. The detector's ability to correctly identify cheater trajectories significantly decreases, as indicated by lower AP and AUROC. Alongside this, we observe a gradual decline in the cheater's average reward. For Gridworld, this trend is closely related to an increase in average trajectory length: As the cheater attempts to appear less suspicious, it avoids taking the most direct and efficient paths to collect items. Instead, it follows longer and less direct routes, similar to the exploratory behavior of non-cheaters, as illustrated in Fig. 6a. For Blackjack, the cheater reduces aggressive behaviors such as surrender or double down. Instead, it adopts more conservative actions that resemble the cautious playstyle of the non-cheater, as shown in Fig. 6b. While these behaviors help the cheater evade detection, they also delay item collection or reduce the bet, resulting in a lower reward.

Interestingly, for small values of $\lambda \leq 0.1$, the detector achieves even higher AP and AUROC than when trained against the pure cheater. During adversarial training, the cheater policy evolves gradually, generating a wide variety of trajectories as it explores different cheating behaviors. This exposes the detector to a more diverse set of training examples compared to the static pure cheater case, allowing it to learn a more robust classifier. However, since the cheater in this case focuses mainly on reward maximization and does not actively attempt to avoid detection, it fails to deceive the improved detector. To support this observation, we present the performance of all combinations of pretrained and adversarially trained cheaters and detectors under $\lambda = 0.01$ in Tab. 3 in the Appendix. The adversarially trained detector outperforms the pretrained one across both AP and AUROC, regardless of the cheater's training method. This suggests that the detector becomes more

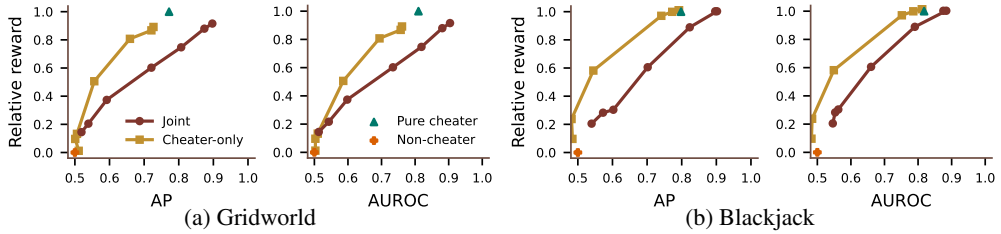


Figure 5: Reward changes over detectability. We can interpret figures from two different perspectives. (1) At an equivalent level of detectability across detectors, the cheater can get less reward with the adversarially trained detector compared to the fixed detector. (2) At an equivalent level of cheater reward, the adversarially trained detector achieves higher detectability than the fixed detector.

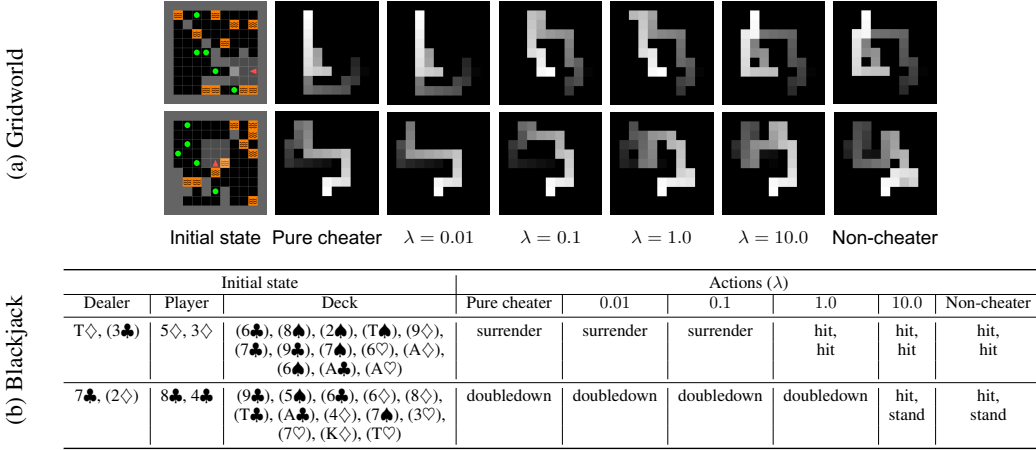


Figure 6: Trajectories generated by cheaters trained under different λ . As λ increases, the cheater tends to avoid optimal behavior and takes less direct paths to stay hidden from the detector.

robust than when trained solely against a pure cheater. For intermediate values $0.1 < \lambda < 1.0$, the cheater achieves better evasion than the pure cheater, but the detector still performs reasonably well, with AP and AUROC remaining above 0.6. In contrast, when $\lambda \geq 1.0$, both AP and AUROC drop to around 0.5-0.6, indicating that the detector can no longer reliably distinguish cheater trajectories from those of non-cheaters. It suggests that the cheater has learned highly deceptive behavior, effectively making the detector useless. Fig. 5 shows that the cheater still achieves a higher average reward than the non-cheater, despite having lower AP and AUROC. Specifically, the adversarially trained cheater retains approximately 30-40% of the reward advantage that the pure cheater has over the non-cheater at an AP and AUROC of 0.6. It demonstrates that the cheater can effectively evade detection while still consistently gaining an advantage over multiple episodes.

4.3 ABLATION STUDIES

To analyze the adaptability of the cheater, we conduct an additional experiment where the detector is kept fixed and only the cheater policy is updated. In Fig. 4, we observe that the overall trends in the average reward and the average trajectory length remain similar to those in the adversarial training setting. However, the overall detection performance is lower than in the adversarial training case. Even when λ is very small ($\lambda = 0.01$), the detection scores remain below the pure cheater's scores. Since the detector does not update, the cheater can repeatedly reinforce its policy in the same direction, leading to a stable reduction in detection scores. As a result, the cheater is able to achieve higher rewards for the same detection score compared to the adversarial training setting, as shown in Fig. 5. It highlights the importance of continuously updating the detector, as a fixed detector may be insufficient to counter adaptive cheaters over time.

Next, we analyze how the design choice of the detector affects detection performance. In addition to the trajectory-based detector used in our main experiments, we use trajectory-length-based and reward-based detectors. Refer to Appendix D for details of detectors. As shown in Fig. 7, the

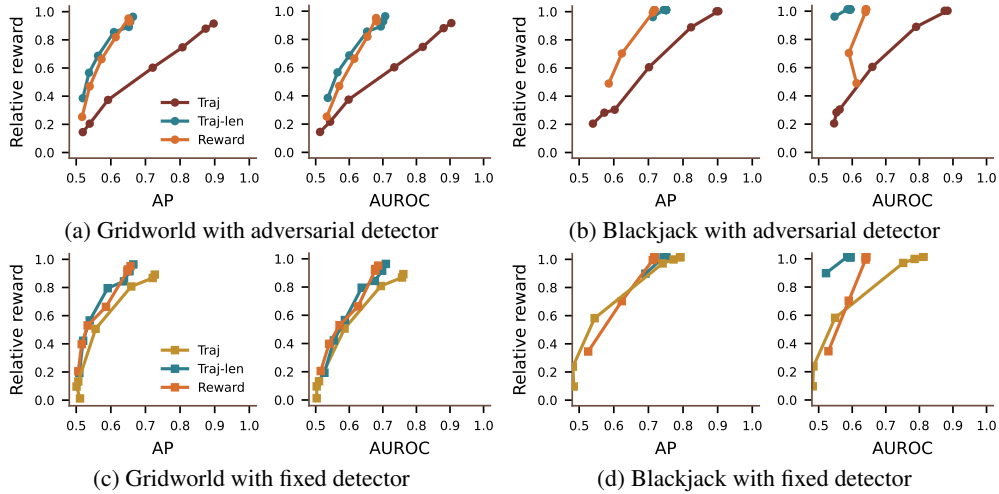


Figure 7: The trajectory-based detector (*Traj*) outperforms both the trajectory-length-based (*Traj-len*) and the reward-based detector (*Reward*) when using adversarially trained detectors. On the other hand, there is not much performance difference between detectors when using fixed detectors.

trajectory-based detector consistently outperforms others when using adversarially trained detectors. It suggests that trajectory information is more effective in identifying cheating behavior than trajectory length or reward alone. In contrast, when using fixed detectors, the performance differences among the three designs are marginal. It highlights that without continuously adapting detectors against evolving cheaters, even a well-designed detector provides limited benefit.

Lastly, we investigate the effect of the structured cheater modeling architecture. We demonstrate that training without the structured modeling may lead to unstable training dynamics, especially when the adversarial pressure is high (i.e., adversarial coefficient λ is large). We provide detailed descriptions and experimental results related to this in Appendix C.

5 CONCLUSIONS AND FUTURE WORKS

In this paper, we present the ESP simulation framework, which models ESP cheaters, non-cheaters, and cheat detectors with their adversarial relationships. Experimental results demonstrate that our framework can effectively simulate adaptive cheater behaviors that balance reward optimization and evade detection. We show that the fixed detector can be easily exploited by adaptive cheaters, emphasizing the need for continuously updated detection mechanisms. We further analyze that the cheater can outperform the non-cheater in terms of average reward, while remaining undetected by a trajectory-based detector. These results suggest that detecting adaptive cheaters may require more sophisticated approaches, such as utilizing behavior patterns observed across multiple episodes.

While this work focuses on simple game environments, we believe it can be extended to more complex settings. First, it would be valuable to experiment with games that involve more intricate rules and strategic decision-making, such as FPS games or multiplayer environments. Studying cheater behavior and detector performance in multiplayer settings would provide more realistic and practical insights for building robust anti-cheat systems. To achieve this, it is necessary to develop a more efficient learning methodology than the current GDA-based approach to shorten the time required for policy training. In this regard, the theoretical analysis of the efficiency, stability, and convergence characteristics of the optimization process would be an important research direction. Next, it would be valuable to check how similar the simulated players are to the real-world players. Regarding this, we have made strong assumptions that both the cheater and non-cheater are single locally optimal players, and the cheater has access to the cheater probability from the detector. In practical scenarios, however, multiple non-optimal players exist, and only binary signals are available from the detector. It could produce a gap between the real and the simulation. Therefore, we plan to extend the framework to include multiple cheaters and non-cheaters at different levels of play, with binary feedback from the detector for a more realistic simulation.

REFERENCES

Leonard Adolphs, Hadi Daneshmand, Aurelien Lucchi, and Thomas Hofmann. Local saddle point optimization: A curvature exploitation approach. In *The 22nd International Conference on Artificial Intelligence and Statistics*, pp. 486–495. PMLR, 2019.

Hashem Alayed, Fotos Frangoudes, and Clifford Neuman. Behavioral-based cheating detection in online first person shooters using machine learning techniques. In *2013 IEEE conference on computational intelligence in games (CIG)*, pp. 1–8. IEEE, 2013.

Carlos Alos-Ferrer and Ana B Ania. Local equilibria in economic games. *Economics Letters*, 70(2):165–173, 2001.

Karl Johan Åström. Optimal control of markov processes with incomplete state information i. *Journal of mathematical analysis and applications*, 10:174–205, 1965.

Wei Chen, Zhenming Liu, Xiaorui Sun, and Yajun Wang. Community detection in social networks through community formation games. In *IJCAI Proceedings-International Joint Conference on Artificial Intelligence*, volume 22, pp. 2576, 2011.

Pengyu Cheng, Tianhao Hu, Han Xu, Zhisong Zhang, Zheng Yuan, Yong Dai, Lei Han, Nan Du, and Xiaolong Li. Self-playing adversarial language game enhances llm reasoning, 2025.

Maxime Chevalier-Boisvert, Bolun Dai, Mark Towers, Rodrigo de Lazcano, Lucas Willems, Salem Lahlou, Suman Pal, Pablo Samuel Castro, and Jordan Terry. Minigrid & miniworld: Modular & customizable reinforcement learning environments for goal-oriented tasks. *CoRR*, abs/2306.13831, 2023.

Giorgio Coricelli and Rosemarie Nagel. Neural correlates of depth of strategic reasoning in medial prefrontal cortex. *Proceedings of the National Academy of Sciences*, 106(23):9163–9168, 2009.

Constantinos Daskalakis and Ioannis Panageas. The limit points of (optimistic) gradient descent in min-max optimization. *Advances in neural information processing systems*, 31, 2018.

Michael Dennis, Natasha Jaques, Eugene Vinitsky, Alexandre Bayen, Stuart Russell, Andrew Critch, and Sergey Levine. Emergent complexity and zero-shot transfer via unsupervised environment design. In *Advances in Neural Information Processing Systems 33*, pp. 13049–13061, 2020. NeurIPS 2020.

Yonathan Efroni, Nadav Merlis, and Shie Mannor. Reinforcement learning with trajectory feedback. In *Proceedings of the AAAI conference on artificial intelligence*, volume 35, pp. 7288–7295, 2021.

Jianqing Fan, Zhaoran Wang, Yuchen Xie, and Zhuoran Yang. A theoretical analysis of deep q-learning. In *Learning for dynamics and control*, pp. 486–489. PMLR, 2020.

Sjur Didrik Flåm. Restricted attention, myopic play, and thelearning of equilibrium. *Annals of Operations Research*, 82(0):59–82, 1998.

Chao Gao, Pablo Hernandez-Leal, Bilal Kartal, and Matthew E Taylor. Skynet: A top deep rl agent in the inaugural pommerman team competition. *arXiv preprint arXiv:1905.01360*, 2019.

Ian Goodfellow, Jean Pouget-Abadie, Mehdi Mirza, Bing Xu, David Warde-Farley, Sherjil Ozair, Aaron Courville, and Yoshua Bengio. Generative adversarial networks. *Communications of the ACM*, 63(11):139–144, 2020.

Sven Gowal, Krishnamurthy Dvijotham, Robert Stanforth, Rudy Bunel, Chongli Qin, Jonathan Uesato, Relja Arandjelovic, Timothy Mann, and Pushmeet Kohli. On the effectiveness of interval bound propagation for training verifiably robust models. *arXiv preprint arXiv:1810.12715*, 2018.

Jonathan Ho and Stefano Ermon. Generative adversarial imitation learning. *Advances in neural information processing systems*, 29, 2016.

Markus Holzleitner, Lukas Gruber, José Arjona-Medina, Johannes Brandstetter, and Sepp Hochreiter. Convergence proof for actor-critic methods applied to ppo and rudder. In *Transactions on Large-Scale Data-and Knowledge-Centered Systems XLVIII: Special Issue In Memory of Univ. Prof. Dr. Roland Wagner*, pp. 105–130. Springer, 2021.

Irdeto. Cheating in video games: The A to Z. <https://irdeto.com/blog/cheating-in-games-everything-you-always-wanted-to-know-about-it>, 2022.

Aditya Jonnalagadda, Iuri Frosio, Seth Schneider, Morgan McGuire, and Joohwan Kim. Robust vision-based cheat detection in competitive gaming. *Proceedings of the ACM on Computer Graphics and Interactive Techniques*, 4(1):1–18, 2021.

Leslie Pack Kaelbling, Michael L Littman, and Anthony R Cassandra. Planning and acting in partially observable stochastic domains. *Artificial intelligence*, 101(1-2):99–134, 1998.

Daniel Kahneman and Amos Tversky. The psychology of preferences. *Scientific american*, 246(1):160–173, 1982.

Anssi Kanervisto, Tomi Kinnunen, and Ville Hautamäki. Gan-aimbots: Using machine learning for cheating in first person shooters. *IEEE Transactions on Games*, 15(4):566–579, 2022.

Diederik P Kingma and Jimmy Ba. Adam: A method for stochastic optimization. *arXiv preprint arXiv:1412.6980*, 2014.

Yang Liu, Yunan Luo, Yuanyi Zhong, Xi Chen, Qiang Liu, and Jian Peng. Sequence modeling of temporal credit assignment for episodic reinforcement learning. *arXiv preprint arXiv:1905.13420*, 2019.

Hamid Maei, Csaba Szepesvari, Shalabh Bhatnagar, Doina Precup, David Silver, and Richard S Sutton. Convergent temporal-difference learning with arbitrary smooth function approximation. *Advances in neural information processing systems*, 22, 2009.

Eric Mazumdar, Lillian J Ratliff, and S Shankar Sastry. On gradient-based learning in continuous games. *SIAM Journal on Mathematics of Data Science*, 2(1):103–131, 2020.

Volodymyr Mnih, Adria Puigdomenech Badia, Mehdi Mirza, Alex Graves, Timothy Lillicrap, Tim Harley, David Silver, and Koray Kavukcuoglu. Asynchronous methods for deep reinforcement learning. In *International conference on machine learning*, pp. 1928–1937. PMLR, 2016.

Rosemarie Nagel. Unraveling in guessing games: An experimental study. *The American economic review*, 85(5):1313–1326, 1995.

Andrew Y Ng, Daishi Harada, and Stuart Russell. Policy invariance under reward transformations: Theory and application to reward shaping. In *International conference on machine learning*, volume 99, pp. 278–287. Citeseer, 1999.

Keiron O’shea and Ryan Nash. An introduction to convolutional neural networks. *arXiv preprint arXiv:1511.08458*, 2015.

José Pedro Pinto, André Pimenta, and Paulo Novais. Deep learning and multivariate time series for cheat detection in video games. *Machine Learning*, 110(11):3037–3057, 2021.

Lerrel Pinto, James Davidson, Rahul Sukthankar, and Abhinav Gupta. Robust adversarial reinforcement learning. In *Proceedings of the 34th International Conference on Machine Learning*, volume 70 of *Proceedings of Machine Learning Research*, pp. 2817–2826. PMLR, 2017.

PUBG: BATTLEGROUNDS Anti-Cheat Team. Dev Letter: ANTI-ESP. <https://pubg.com/en/news/6957>, 2024.

Lillian J Ratliff, Samuel A Burden, and S Shankar Sastry. On the characterization of local nash equilibria in continuous games. *IEEE transactions on automatic control*, 61(8):2301–2307, 2016.

John Schulman, Philipp Moritz, Sergey Levine, Michael Jordan, and Pieter Abbeel. High-dimensional continuous control using generalized advantage estimation. *arXiv preprint arXiv:1506.02438*, 2015.

John Schulman, Filip Wolski, Prafulla Dhariwal, Alec Radford, and Oleg Klimov. Proximal policy optimization algorithms. *arXiv preprint arXiv:1707.06347*, 2017.

Reinhard Selten. Bounded rationality. *Journal of Institutional and Theoretical Economics (JITE)/Zeitschrift für die gesamte Staatswissenschaft*, 146(4):649–658, 1990.

Herbert A Simon. A behavioral model of rational choice. *The quarterly journal of economics*, pp. 99–118, 1955.

Shan Suthaharan. Support vector machine. In *Machine learning models and algorithms for big data classification: thinking with examples for effective learning*, pp. 207–235. Springer, 2016.

Jianrong Tao, Jiarong Xu, Linxia Gong, Yifu Li, Changjie Fan, and Zhou Zhao. Nguard: A game bot detection framework for netease mmorpgs. In *Proceedings of the 24th ACM SIGKDD international conference on knowledge discovery & data mining*, pp. 811–820, 2018.

Haoxing Tian, Alex Olshevsky, and Yannis Paschalidis. Convergence of actor-critic with multi-layer neural networks. *Advances in neural information processing systems*, 36:9279–9321, 2023.

Valve. Counter-Strike: Global offensive. <https://blog.counter-strike.net>, 2012.

Jiayi Zhang, Chenxin Sun, Yue Gu, Qingyu Zhang, Jiayi Lin, Xiaojiang Du, and Chenxiong Qian. Identify as a human does: A pathfinder of next-generation anti-cheat framework for first-person shooter games. *arXiv preprint arXiv:2409.14830*, 2024.

Grid size	Agent's view size	# items	# walls	# lava	Maximum episode length
11×11	3×3	5	10	10	484

Table 2: Default configuration of the Gridworld environment.

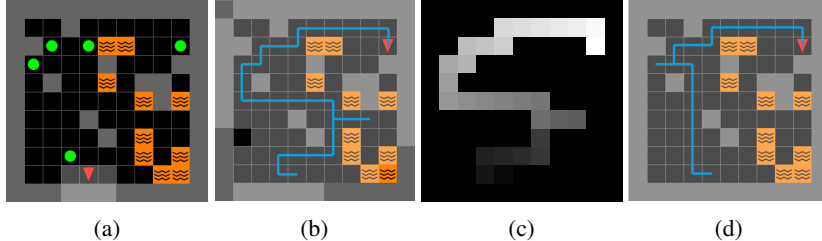


Figure 8: Visualizations of the Gridworld environment and the agent behavior. The figures show walls in gray, the agent as a red triangle, collectible items as green circles, and lava as orange regions with black wave patterns. (a) Initial state and observation: Only the 3×3 region in front of the agent is visible. (b) Retrospective board and the movement history (Non-cheater): Light-colored tiles represent areas that have been observed by the agent. The blue line traces the agent's history throughout the episode. (c) History heatmap: A heatmap of the agent's movement over time, with brighter colors indicating more recent positions. (d) Retrospective board and the movement history (Cheater): All tiles are visible, even for areas the agent has not approached.

A ENVIRONMENT DETAILS

A.1 GRIDWORLD

Environment Layout. Gridworld environment is a two-dimensional grid world based on the Min-iGrid (Chevalier-Boisvert et al., 2023) framework. It contains $n \times n$ tiles, surrounded by walls that prevent the agent from leaving the environment. At the beginning of each episode, we randomly place the agent with a random facing direction. We also randomly distribute the collectible items, the walls, and the lava across empty cells. Fig. 8a shows the example of the initial state and the initial observation for the agents. The episode ends when the agent has collected all items or the maximum number of timesteps has elapsed.

The agent interacts with the environment through a discrete action space \mathcal{A} , consisting of three primitive actions: *TurnLeft*, *TurnRight*, and *MoveForward*. These actions control the agent's orientation and position within the grid. When the agent executes *MoveForward* and enters a tile containing an item, the item is immediately collected and removed from the environment. Upon collecting the item, the agent receives $1 - t/T$ as a reward, where t is the current timestep and T is the maximum length of the episode. This time-decaying reward encourages the agent to collect items as quickly as possible. When the agent steps into a lava tile, the lava is removed, and the agent receives a time-decaying penalty of $-0.1 \times (1 - t/T)$, discouraging such behavior. Tab. 2 summarizes the default environment configurations used throughout our experiments.

Input Structures. The cheater and the non-cheater receive observation dictionaries consisting of five components: *Agent view*, *Movement history*, *Retrospective board*, *Item*, and *Time*. *Agent view* provides a top-down visual representation of the environment from the agent's perspective at the current timestep. Only a small square region in front of the agent is visible to them. *Movement history* is represented as a heatmap that records the agent's movement over time; each cell stores the timestep at which the agent last visited that location, with unvisited cells set to zero. We normalize the recorded timestep values to the range $[0, 1]$, where higher values correspond to more recent visits. Fig. 8c is an example of the movement history heatmap. *Retrospective board* (Gao et al., 2019) is a global memory map that records the latest observed information for each tile. Whenever a tile becomes visible to the agent, the retrospective board is updated accordingly. Non-cheater agents can only access their own partially constructed retrospective board based on their observations, whereas cheater agents have access to the full environment without any visibility restrictions. Fig. 8b and 8d

	Initial Hand	Deck / Action		Initial Hand	Deck / Action
Dealer	T◊, (3♣)	(6♦), (8♠), (2♦), (T♣), (9◊), (7♣), (9♣), (7♣), (6◊), (A◊), (6♣), (A♣), (A◊)		Dealer	6♦, (8♠), (2♦), (T♣), (9◊), (7♣), (9♣), (7♣), (6◊), (A◊), (6♣), (A♣), (A◊)
Player	5◊, 3◊			Player	5◊, 3◊

(a) Initial state

(b) Final state

Figure 9: Visualizations of the Blackjack environment. Cards with the parenthesis are invisible to the non-cheater. (a) is the example initial state and (b) is its final state. Player can only see their hand (initial hand + revealed cards from the deck), dealer’s upcard, and the player’s action history.

illustrate examples of the retrospective board constructed by the non-cheater and the cheater agent. *Item* denotes the number of items collected by the agent, and *Time* indicates the current timestep within the episode.

For the cheat detector, we encode each trajectory as a two-channel image. The first channel represents the agent’s movement history in the form of a heatmap. The second channel captures the initial state of the board, including items, walls, and lava.

A.2 BLACKJACK

Environment Layout. Blackjack is a famous card game played with standard playing cards. The player aims to hold cards whose count does not exceed 21 while exceeding the dealer’s count. The game uses a standard 52-card deck. Card values are as follows: cards from 2 to 9 take their numeric values, 10, J, Q, and K count as 10, and A counts as either 1 or 11.

Before the game starts, the player places a unit bet of 1. The player and the dealer then receive two cards each. The dealer reveals one upcard and keeps one hold card hidden. For each turn, the player can choose one of the actions: *Hit*, *Stand*, *DoubleDown*, and *Surrender*. *Hit* draws one additional card. *Stand* stops drawing card. *DoubleDown* doubles the bet, takes exactly one more card, and then stands. *Surrender* loses half of the bet and finishes the game immediately. To ensure that it is only available at the first turn, the player loses immediately and forfeits two times of the bet if they *Surrender* after the first turn. If the player’s hand exceeds 21 after *Hit* and *DoubleDown*, the player also loses immediately and forfeits the entire bet.

Once the player stops drawing, the dealer reveals the hole card and draws until the total count reaches at least 17. If the dealer’s total count exceeds 21 or is lower than the player’s total count, the player wins and gains an amount equal to the bet. If the player wins with an initial hand of A and a 10-valued card, they receive 1.5 times the bet. If two total counts are equal, then the player gains nothing. Otherwise, the player loses the bet.

Input Structures. The cheater and the non-cheater receive observation consisting of five components: *Player’s initial hand*, *Dealer’s initial hand*, *Deck*, *Player’s current count*, and *Player’s action history*. Fig. 9 illustrates example game states with the observation. Each card in each component is encoded as a pair of its numeric value and a boolean flag that marks whether it is an A. Any card that is not currently visible to the player is masked with 0. After the player chooses *Hit* or *DoubleDown*, the top face-down card of the deck is revealed to the player. On the other hand, the cheater can observe every card, including the dealer’s hole card and the entire deck. The cheat detector receives the same information as the cheater.

B EXPERIMENT SETTING DETAILS

We conducted all experiments on a machine with AMD EPYC 7742 (64-core), NVIDIA A100 (40GB) and 128GB of RAM. We use a CNN-based actor-critic architecture for the policy network and a CNN-based classifier for the detector network. Both the cheater and non-cheater policies are trained using Proximal Policy Optimization (PPO) algorithm (Schulman et al., 2017), with Generalized Advantage Estimation (GAE) (Schulman et al., 2015). We set the GAE parameter to 0.95, the clipping range to 0.2, and the value function loss coefficient to 0.5. We perform the training

	AP		AUROC	
	Detector (Pre.)	Detector (Adv.)	Detector (Pre.)	Detector (Adv.)
Pure cheater	0.760	0.934	0.800	0.939
Cheater (Adv.)	0.733	0.905	0.774	0.911

Table 3: Pretrained (*Pre.*) and adversarially trained (*Adv.*) cheaters and detectors under $\lambda = 0.01$ in the Gridworld environment. Since the cheater’s rewards are very similar, we ignore the reward component and only consider the detectability component when computing the equilibrium. Bold values indicate the equilibrium, where both cheaters and detectors are adversarially trained.

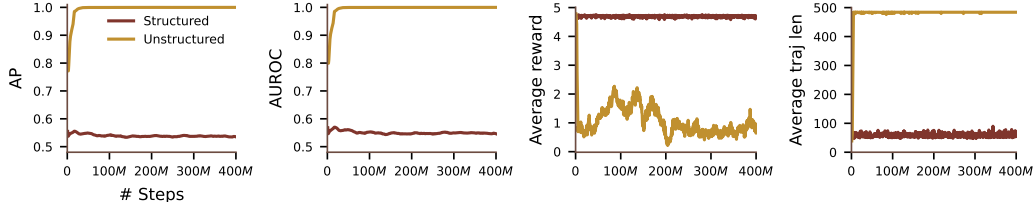


Figure 10: Effect of the structured cheater modeling in the Gridworld environment. We compare two settings under a fixed adversarial coefficient of $\lambda = 3.0$: one using the structured cheater modeling (*Structured*) and one using a standard, unstructured modeling (*Unstructured*). The unstructured modeling exhibits unstable reward patterns and inefficiently long trajectories throughout training. These results indicate that the structured modeling enables the cheater to learn more stably and effectively under strong adversarial pressure.

using 64 parallel environments, each generating rollouts of 2048 steps. PPO updates are applied over 4 epochs with a minibatch size of 1024. An entropy coefficient of 0.01 is used to encourage exploration. As for the detector, it is trained with a batch size of 8. We optimize both the policy and the detector networks using Adam optimizer (Kingma & Ba, 2014) with hyperparameters $\beta_1 = 0.9$, $\beta_2 = 0.999$, and a learning rate of 3×10^{-4} .

Before conducting adversarial training, we pretrain both the policy and detector networks. We pretrain the policies over one billion environment timesteps, and select checkpoints that maximize the reward. For the detector, we construct a trajectory dataset consisting of 10k training samples, 2k validation samples, and 2k test samples for each policy. We then pretrain the detector for 100 epochs and select the checkpoint with the lowest validation loss. The cheater and non-cheater policies were pretrained in about 2.5 days, and the detector was pretrained in roughly 10 minutes. The pretraining results are summarized in Tab. 1.

For adversarial training, we finetune the cheater policy and the detector network for an additional 400 million environment timesteps based on Alg. 1. The adversarial training phase took approximately 3 days. After training, we use the final checkpoints for performance evaluation.

To ensure the reliability of results, we conducted each experiment three times using different random seeds and reported the mean and the standard deviation.

C STRUCTURED CHEATER MODELING STABILIZES TRAINING DYNAMICS

In this section, we compare the training dynamics of the cheater policies with the structured modeling and without employing the structured modeling. We design an unstructured modeling structure as only pure cheater network in Fig. 2. For the comparison, we set $\lambda = 3.0$ to highlight the stability issue that arises during training under strong adversarial pressure. As shown in Fig. 10, the structured modeling consistently maintains high average rewards and short, stable trajectories throughout training. In contrast, the unstructured modeling exhibits highly unstable reward patterns and significantly longer trajectories, indicating inefficient and erratic behavior. This erratic behavior makes the cheater’s actions more distinguishable from those of non-cheaters, leading the detector to classify them with higher confidence. As a result, the detection performance for the unstructured modeling converges to near-perfect levels, with AP and AUROC approaching 1.0.

		Trajectory-length-based detector		Reward-based detector	
Game	Player type	AP	AUROC	AP	AUROC
Gridworld	Pure cheater	0.684 ± 0.002	0.730 ± 0.003	0.675 ± 0.000	0.702 ± 0.005
Blackjack	Pure cheater	0.752 ± 0.003	0.595 ± 0.011	0.717 ± 0.004	0.640 ± 0.005

Table 4: AP and AUROC of the pretrained agents with different detectors.

D EFFECT OF DETECTOR DESIGN

Feature engineering (i.e., selecting important features) plays a crucial role in cheat detection (Alayed et al., 2013). Detector performance can be changed significantly depending on the selected features. Previously, we used the trajectory as a feature to implement the detector. Alternatively, we could use different features such as trajectory length and reward.

In this section, we introduce two additional detectors: a trajectory-length-based detector and a reward-based detector. We design the detectors to reflect the fact that cheaters tend to have shorter trajectory lengths and larger rewards compared to non-cheaters. Therefore, the cheater probability of the trajectory-length-based detector $D_{len} : \mathbb{R} \rightarrow [0, 1]$ and the cheater probability of the reward-based detector $D_{rew} : \mathbb{R} \rightarrow [0, 1]$ can be defined as following logistic functions:

$$D_{len}(l) = \frac{1}{1 + e^{-(l - b_{len})/t_{len}}}, \quad D_{rew}(r) = \frac{1}{1 + e^{-(r - b_{rew})/t_{rew}}}, \quad (8)$$

where l is a trajectory length, r is a reward, t_{len} , b_{len} , t_{rew} and b_{rew} are learnable parameters.

Note that the trajectory length and the reward are not effective criteria for distinguishing cheaters from non-cheaters. It is because their values can vary widely depending on the objects' placement on the map or the values of the cards. As a result, detectors based on these measures achieve much lower AP and AUROC than the trajectory-based detector (Fig. 7a and 7b). Furthermore, cheaters can easily bypass the detectors due to their poor performance. In this case, cheaters can maintain low detectability while obtaining sufficiently high rewards even without considering the detector. Consequently, when the adversarial coefficient λ is not large, metrics remain relatively stable in Fig. 11. In addition, it narrows the performance gap between training with and without the detector, as shown in Fig. 12, compared to what we observed with the trajectory-based detector in Fig. 5.

Except for these points, we observed a trend similar to that of the trajectory-based detector. As λ increases, the cheater policy becomes more difficult to detect, resulting in lower AP and AUROC. To evade the detector, cheaters increase their trajectory length by taking longer and less direct routes. It also delays item collection in Gridworld or reduces the bet in Blackjack, leading to a lower reward.

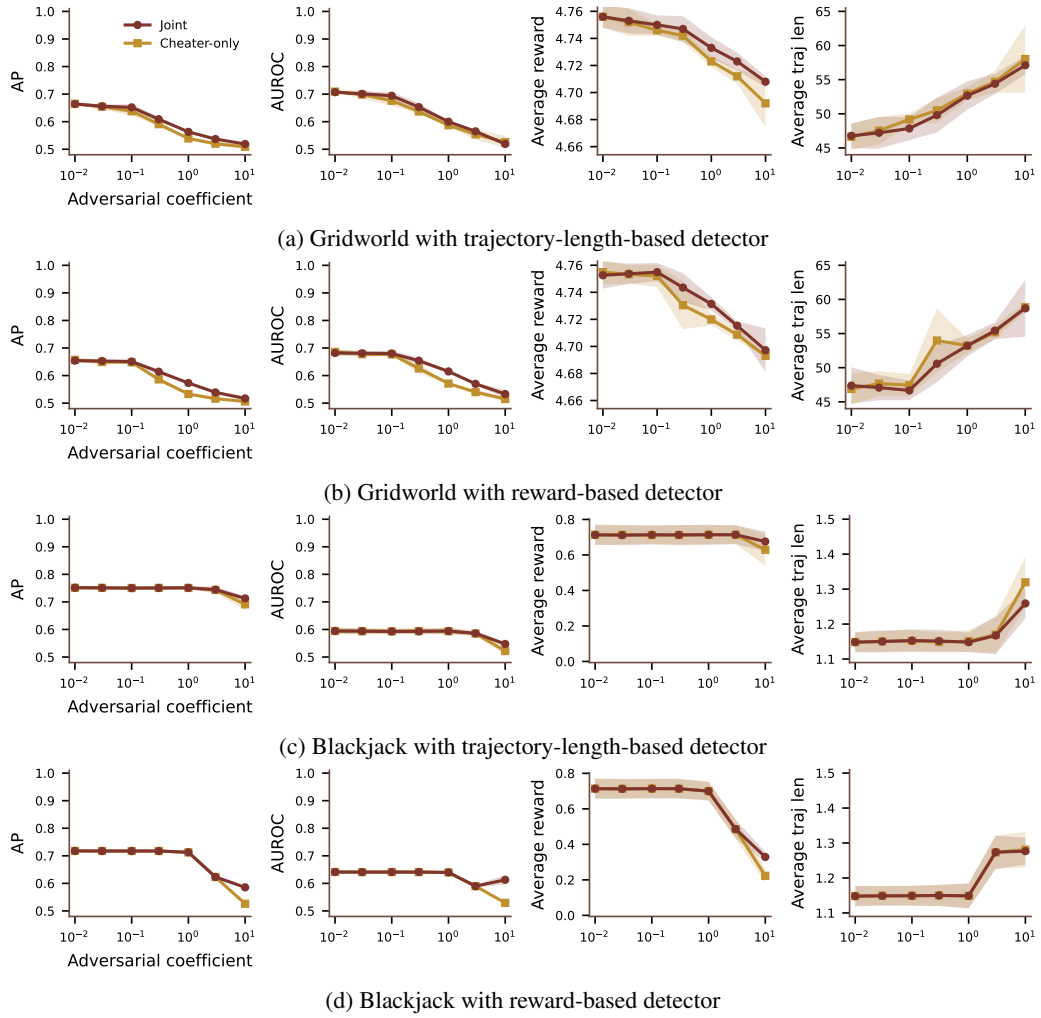


Figure 11: Performance metrics as functions of the adversarial coefficient λ .

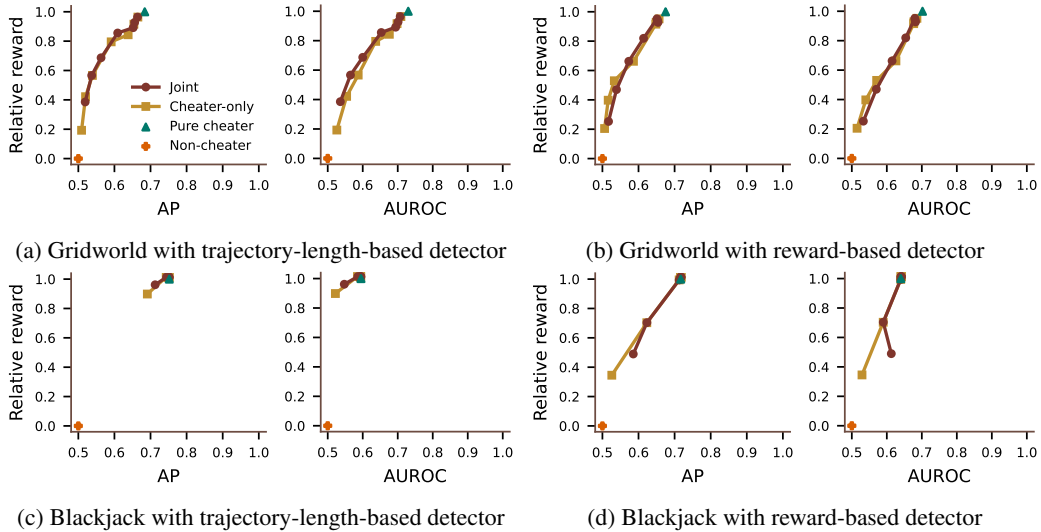


Figure 12: Reward changes over detectability.